

Hypernuclei production in Pb–Pb collisions at $\sqrt{s_{NN}} = 2.76$ TeV with ALICE at the LHC

Ramona Lea,¹ for the ALICE Collaboration

Physics Department, University and INFN of Trieste, Via A. Valerio 2, 34127 Trieste, Italy

Received 12 December 2012; received in revised form 21 February 2013; accepted 22 February 2013

Available online 5 March 2013

Abstract

Results on (anti)hypertriton production in Pb–Pb collisions at $\sqrt{s_{NN}} = 2.76$ TeV are reported using the data samples collected by the ALICE experiment during the LHC heavy-ion runs at the end of 2011.

The (anti) $^3_{\Lambda}$ H signal is extracted from the study of its mesonic decay ($^3_{\Lambda}\text{H} \rightarrow ^3\text{He} + \pi^-$) via the topological identification of secondary vertices.

The ($^3\text{He}/^3\overline{\text{He}}, \pi$) invariant mass distributions in different transverse momentum intervals are shown.

© 2013 CERN. Published by Elsevier B.V. All rights reserved.

Keywords: Hypertriton; Heavy-ion collisions

1. Introduction

Ultra-relativistic heavy-ion collisions provide a unique opportunity for understanding the strong interaction: many strange hadrons are produced in the collision and the study of their production yield helps to understand the nature of the space–time evolution and chemical equilibrium. In heavy-ion collisions hyperon–baryon bound systems, called hypernuclei [1], can be produced. It is possible to discriminate two distinct mechanisms for hypernuclei formation in heavy-ion collisions: i) the absorption of hyperons in the spectator fragments of non-central collisions (but this mechanism is not important for the measurement at ALICE); or ii) hypernuclei can emerge from the hot and dense fireball region of the reaction. In the latter scenario the cluster is formed at, or shortly after, the (chemical) freeze-out of the system. To estimate the

E-mail address: ramona.lea@ts.infn.it (R. Lea).

¹ © CERN for the benefit of the ALICE Collaboration.

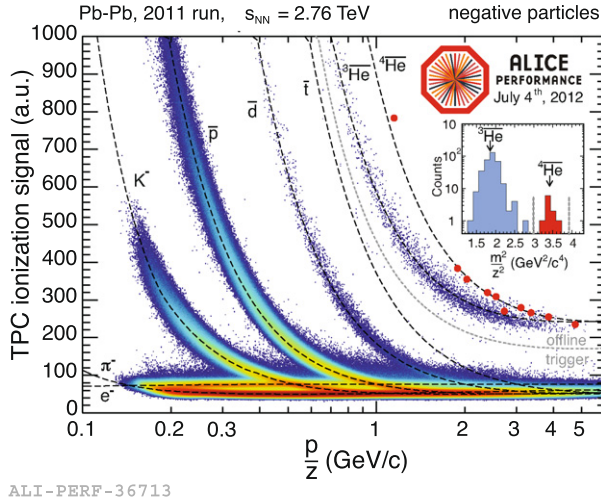


Fig. 1. (dE/dx) in the TPC versus rigidity $R = p/z$ for negative tracks with Bethe–Bloch curves superimposed. Nearly 23 millions of central, semi-central and minimum-bias events have been used to obtain the figure. An offline trigger that selects events with at least a ${}^3\overline{\text{He}}$ or a heavier particle has been applied. The effect of the offline trigger is to enhance the sample of $Z = 2$ particle, while light nuclei with $Z = 1$ are suppressed. In the inlet the m^2/z^2 distribution for all tracks within a 2σ band around the expected dE/dx for ${}^4\overline{\text{He}}$ is shown. For the m^2/z^2 distribution the Time of Flight (TOF) detector has been used. The 10 identified ${}^4\overline{\text{He}}$ are spotted both in m^2/z^2 and in the dE/dx versus rigidity plot.

production yield it is possible to employ either a transport model which equips the coalescence mechanism [2] or a thermal model [3]. The study of the production yield of hypernuclei helps for understanding the particle production mechanisms in heavy-ion collisions.

The production of (anti)(hyper)nuclei with atomic mass $A = 3$ is favoured with respect to nuclei with $A = 4$ according to both the coalescence and the thermal model; studies on systems with $A = 3$ are experimentally achievable with the statistics collected by the ALICE experiment.

The (anti)hypertriton (${}^3_{\Lambda}\overline{\text{H}}$) ${}^3_{\Lambda}\text{H}$ is the lightest known hypernucleus and is formed from an (anti)proton, an (anti)neutron and an (anti) Λ . ${}^3_{\Lambda}\text{H}$ decays mesonically into the following channels [4]:

$${}^3_{\Lambda}\text{H} \rightarrow \pi^- (\pi^0) + {}^3\text{He} ({}^3\text{H}) \quad B.R. = (30\text{--}39)\% \quad (1)$$

$${}^3_{\Lambda}\text{H} \rightarrow \pi^- (\pi^0) + d + p(n) \quad B.R. = (51\text{--}69)\% \quad (2)$$

$${}^3_{\Lambda}\text{H} \rightarrow \pi^- (\pi^0) + p + n + p(n) \quad B.R. \leq 10\% \quad (3)$$

The study of the production of (${}^3_{\Lambda}\overline{\text{H}}$) ${}^3_{\Lambda}\text{H}$ detected via its decay ${}^3_{\Lambda}\text{H} \rightarrow {}^3\text{He} + \pi^-$ (${}^3_{\Lambda}\overline{\text{H}} \rightarrow {}^3\overline{\text{He}} + \pi^+$) using the ALICE experiment is presented here. In Section 2 the analysis method is described, then in Section 3 the results are summarized.

2. Analysis

For the present study, nearly 23 million of central, semi-central and minimum-bias events from Pb–Pb collisions at $\sqrt{s_{NN}} = 2.76$ TeV collected by ALICE [5,6] during the 2011 run are analyzed. The main detector used in the analysis is the Time Projection Chamber (TPC) [7] which has a full azimuthal acceptance for tracks in the pseudo-rapidity region $|\eta| < 0.9$. Fig. 1 shows the

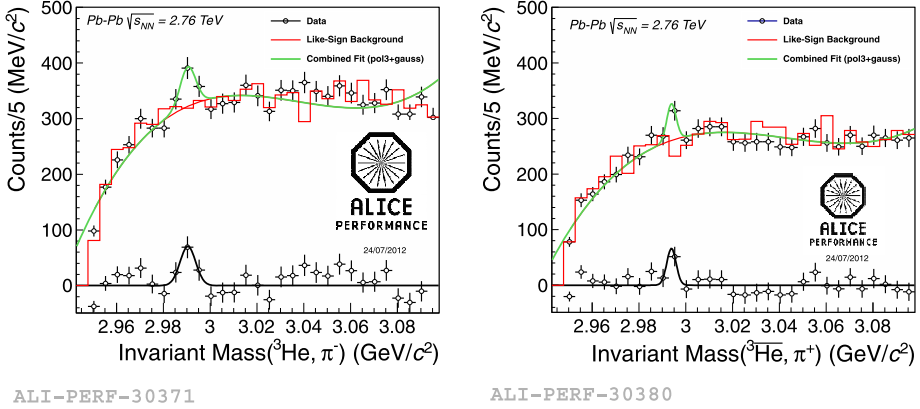


Fig. 2. a) $({}^3\text{He}, \pi^-)$ invariant mass distribution, b) $({}^3\overline{\text{He}}, \pi^+)$ invariant mass distribution. The distributions are fitted with a function which is the sum of a third degree polynomial and a Gaussian (light curve). Empty circle points are $({}^3\text{He}, \pi^-)$ ($({}^3\overline{\text{He}}, \pi^+)$) invariant mass distribution, while the full line is the “like-sign” $({}^3\text{He}, \pi^+)$ ($({}^3\overline{\text{He}}, \pi^-)$) invariant mass distribution.

measured specific energy loss (dE/dx) versus rigidity $R = p/z$, where p is the track momentum and z is the charge number, for negative tracks when an offline trigger, that selects events with at least a ${}^3\overline{\text{He}}$ or a heavier particle, has been applied. The superimposed lines are Bethe–Bloch curves for the different particle species. The figure has been produced using the full statistics of the 2011 data taking. In the inlet the m^2/z^2 distribution for all tracks within a 2σ band around the expected dE/dx for ${}^4\overline{\text{He}}$ is shown. Information from the Time of Flight (TOF) [6] detector has been used to obtain m^2/z^2 , according to the relation $m^2/z^2 = R^2/\gamma^2 - 1$.

The 10 identified ${}^4\overline{\text{He}}$ are spotted both in m^2/z^2 and in the dE/dx versus rigidity plot.

Both daughter particles of the $({}^3_{\Lambda}\overline{\text{H}}) {}^3_{\Lambda}\text{H}$ can be identified using the TPC over a wide range of momentum.

Once both daughter tracks are identified, it is possible to reconstruct the hypertriton signal candidates by reconstructing their decay vertices. A set of topological cuts has been implemented in order to reduce the combinatorial background. These cuts include: the Distance of Closest Approach (DCA) between the two tracks (<0.7 cm), the DCA of the negative track from the primary vertex (>0.4 cm) and the cosine of the pointing angle between the line joining the primary and secondary vertex and the total momentum vector direction (>0.9).

Using the 2011 statistics it has been possible to obtain a ${}^3_{\Lambda}\text{H}$ (${}^3_{\Lambda}\overline{\text{H}}$) signal. The left panel of Fig. 2 shows the invariant mass distribution of $({}^3\text{He}, \pi^-)$, while the right panel of Fig. 2 shows the invariant mass distribution of $({}^3\overline{\text{He}}, \pi^+)$: empty circle points are the $({}^3\text{He}, \pi^-)$ ($({}^3\overline{\text{He}}, \pi^+)$) invariant mass distribution, while the full line is the “like-sign” $({}^3\text{He}, \pi^+)$ ($({}^3\overline{\text{He}}, \pi^-)$) invariant mass distribution; the light curve is a function which is the sum of a third order polynomial, used to evaluate the combinatorial “like-sign” background, and a Gaussian used to describe the signal. The black line in the lower part of the plot is the signal extracted after the polynomial background subtraction.

From the combined fit it is possible to evaluate the invariant mass (μ), the width (σ) and the raw yield, both for ${}^3_{\Lambda}\text{H}$ and ${}^3_{\Lambda}\overline{\text{H}}$ candidates.

Using the information of the fit, the mean for the ${}^3_{\Lambda}\text{H}$ signal is $\mu = 2.990 \pm 0.001$ GeV/ c^2 , the width $\sigma = (3.35 \pm 0.7) \times 10^{-3}$ GeV/ c^2 and the raw yield is $N_{\text{raw}} = 119 \pm 35$. For the ${}^3_{\Lambda}\overline{\text{H}}$, the mean is $\mu = 2.993 \pm 0.001$ GeV/ c^2 , the width $\sigma = (2.00 \pm 1.2) \times 10^{-3}$ GeV/ c^2

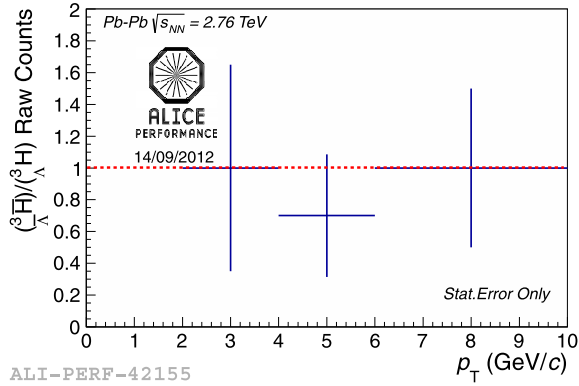


Fig. 3. $\frac{{}^3\text{H}}{{}^3\bar{\text{H}}}$ ratio of raw yields versus p_T : this ratio is consistent with unity (reference line) in the whole p_T range. Uncertainties are statistical only.

and the raw yield is $N_{\text{raw}} = 77 \pm 22$. The significance of each signal, when calculated as $\text{Significance} = S/\sqrt{S+B}$, where S is the value of the signal integral and B the one of the background, is 4.6 and 3.6. The obtained widths are primarily related to the detector performances, and are consistent with the ones obtained from the simulations.

The 2011 statistics allows to extract a $\frac{{}^3\text{H}}{{}^3\bar{\text{H}}}$ signal in 3 p_T bins: $2 \leq p_T < 4$ GeV/ c , $4 \leq p_T < 6$ GeV/ c and $6 \leq p_T < 10$ GeV/ c . The same procedure to extract the signal described in the previous paragraph has been applied for each p_T bin, both for $({}^3\text{He}, \pi^-)$ and $({}^3\bar{\text{H}}, \pi^+)$ invariant mass distributions.

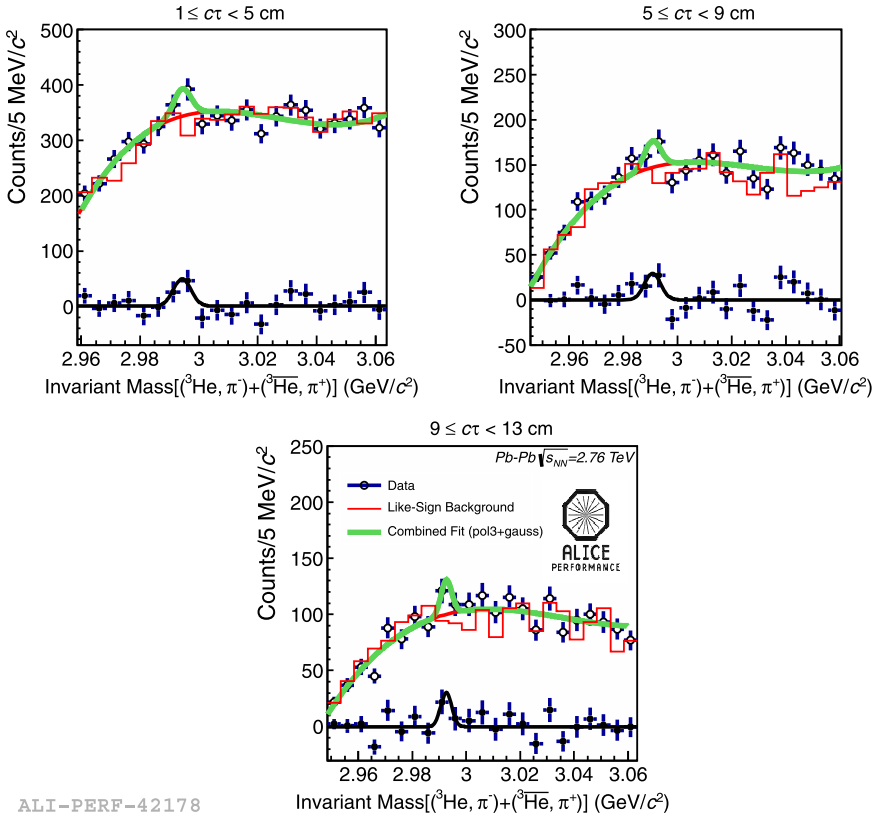
Quality checks on the stability of the mean and the width of the $\frac{{}^3\text{H}}{{}^3\bar{\text{H}}}$ have been done. The width versus p_T is stable, the mean is stable (variation $< 0.5\%$) and consistent with the value of $\frac{{}^3\text{H}}$ mass from literature [8].

Fig. 3 shows the $\frac{{}^3\text{H}}{{}^3\bar{\text{H}}}$ ratio of the raw yields versus p_T : this ratio is consistent to unity (reference line) in the whole p_T range considered.

Using the statistics recorded in 2011 it has also been possible to extract the $(\frac{{}^3\text{H}}{{}^3\bar{\text{H}}})$ signal in three $c\tau$ bins, where $c\tau$ has been defined as $c\tau = \frac{ML}{p}$, where M is the nominal value of the $\frac{{}^3\text{H}}$ mass = 2.991 GeV/ c^2 , L is the decay length and p is the total momentum of the $\frac{{}^3\text{H}}$ candidate. Fig. 4 shows the invariant mass spectrum of the sum of $\frac{{}^3\text{H}}$ and $\frac{{}^3\bar{\text{H}}}$ candidates relative to 3 different $c\tau$ bins: $1 \leq c\tau < 5$ cm (top left panel), $5 \leq c\tau < 9$ cm (top right panel), and $9 \leq c\tau < 13$ cm (bottom panel). The empty circle points are the $(({}^3\text{He}, \pi^+) + ({}^3\bar{\text{He}}, \pi^-))$ invariant mass distribution, while full line is the “like-sign” invariant mass spectrum. The light curve is a function which is the sum of a third degree polynomial, used to evaluate the “like-sign” combinatorial background, and a Gaussian for the signal. The full line in the lower part of the plot is the signal extracted after the polynomial background subtraction. A signal is clearly visible in each panel. As soon as the efficiency correction is available the $\frac{{}^3\text{H}}$ lifetime can be determined.

3. Summary

The invariant mass distributions of $({}^3\text{He}, \pi^-)$ and $({}^3\bar{\text{He}}, \pi^-)$ have been studied using nearly 23 millions of central, semi-central and minimum-bias Pb–Pb collisions at $\sqrt{s_{\text{NN}}} = 2.76$ TeV, and a $(\frac{{}^3\bar{\text{H}}}) \frac{{}^3\text{H}}$ signal was found.



ALI-PERF-42178

Fig. 4. [$({}^3\text{He}, \pi^-) + ({}^3\bar{\text{He}}, \pi^+)$] invariant mass spectra for 3 $c\tau$ bins. a) [1–5] cm, b) [5–9] cm, c) [9–13] cm. The distributions are fitted with a function which is the sum of a third degree polynomial and a Gaussian function (light curve). Empty circle points are $(({}^3\text{He}, \pi^+) + ({}^3\bar{\text{He}}, \pi^-))$ invariant mass distribution while the full line is the “like-sign” (LS) invariant mass distribution.

${}^3_{\Lambda}\text{H}$ and ${}^3_{\Lambda}\bar{\text{H}}$ signals have been extracted in 3 p_T bins: the mean is stable (variation $<0.5\%$) and consistent with the value from the literature [8], and also the sigma is stable. The ${}^3_{\Lambda}\text{H}/{}^3_{\Lambda}\bar{\text{H}}$ raw ratio is consistent with unity.

The $({}^3_{\Lambda}\text{H} + {}^3_{\Lambda}\bar{\text{H}})$ signal has been extracted also in 3 $c\tau$ bins.

The work on efficiency correction and the evaluation of the systematic uncertainties is ongoing.

Open access

This article is published Open Access at sciencedirect.com. It is distributed under the terms of the Creative Commons Attribution License 3.0, which permits unrestricted use, distribution, and reproduction in any medium, provided the original authors and source are credited.

References

[1] M. Danysz, J. Pniewski, Phil. Mag. 44 (1953) 348;

- B. Povh, *Annu. Rev. Nucl. Part. Sci.* 28 (1978) 1–32.
- [2] J. Steinheimer, et al., *Phys. Lett. B* 714 (2012) 85.
- [3] A. Andronic, et al., *Phys. Lett. B* 697 (2011) 203.
- [4] D. Bertrand, et al., *Nucl. Phys. B* 16 (1970) 77–84;
G. Keyes, et al., *Phys. Rev. D* 1 (1970) 66;
G. Keyes, et al., *Phys. Rev. Lett.* 20 (1968) 819;
G. Keyes, et al., *Nucl. Phys. B* 67 (1973) 269.
- [5] K. Aamodt, et al., ALICE Collaboration, *J. Phys. G: Nucl. Part. Phys.* 32 (2006) 1295.
- [6] K. Aamodt, et al., ALICE Collaboration, *JINST* 3 (2008).
- [7] J. Alme, et al., *Nucl. Instrum. Meth. A* 622 (2010) 316–367.
- [8] M. Juric, et al., *Nucl. Phys. B* 52 (1973) 1.